



Flexible fluorinated graphite foils with high content of $(C_2F)_n$ phase for slow neutron reflector

Journal:	<i>Dalton Transactions</i>
Manuscript ID	DT-ART-03-2024-000794.R1
Article Type:	Paper
Date Submitted by the Author:	01-May-2024
Complete List of Authors:	Henry, Killian; Institut Jean Lamour Colin, Marie; Université Clermont Auvergne Chambery, Gabin; Université Clermont Auvergne Vigolo, Brigitte; Institut Jean Lamour Cahen, Sébastien; Institut Jean Lamour Hérold, Claire; Institut Jean Lamour Nesvizhevsky, Valery; Institut Laue-Langevin Le Floch, Sylvie; CNRS, Institut Lumière Matière-UMR 5306-CNRS- Université Lyon1 CNRS; Institut Lumière Matière-UMR 5306--UCBL Lyon1 CNRS Pischedda, Vittoria; CNRS, Institut Lumière Matière-UMR 5306-CNRS- Université Lyon1 CNRS 10 rue Ada Byron Campus LyonTech La doua-bat. Kastler Villeurbanne cedex, FR 69622 Chen, Xianjue; The University of Newcastle Dubois, Marc; University of Clermont Auvergne,

ARTICLE

Flexible fluorinated graphite foils with high content of (C₂F)_n phase for slow neutron reflector

Received 00th January 20xx,
Accepted 00th January 20xx

Killian Henry^{a,b}, Marie Colin^a, Gabin Chambéry^a, Brigitte Vigolo^b, Sébastien Cahen^{b,*}, Claire Hérold^b, Valery Nesvizhevsky^c, Sylvie Le Floch^d, Vittoria Pischcedda^d, Sam Chen^e, Marc Dubois^a

DOI: 10.1039/x0xx00000x

In order to prepare self-standing and flexible slow neutrons reflectors made with graphite fluoride (GF) of high content of (C₂F)_n structural phase, graphite foils of different thicknesses were used as starting material for the gas (F₂)/solid fluorination. The maximal interlayer distance for GF was obtained with this phase thanks to a stacking sequence FCCF/FCCF; this is mandatory for the efficient reflection of slow neutrons. 71 and 77 % of (C₂F)_n phase were achieved for graphite foils with thicknesses of 1.0 and 0.1 mm, respectively. The interlayer distances were then of 8.6 Å as expected. The fluorination conditions (static mode, long duration of 24 h and annealing in pure F₂ gas for 24 h, temperatures in the 390-460 °C range) were adapted to large pieces of graphite foils (7x7 cm²) in order to both avoid the exfoliation and achieve a homogenous dispersion of fluorine atoms. This process was also efficient for thinner (0.01 mm of thickness) graphitized graphene oxide afoil. 56 % of (C₂F)_n phase and interlayer of 8.6 Å were achieved for this foil when the fluorination was performed at 430°C. Whatever the nature and the thickness of the foil, their flexibilities are maintained.

Introduction

Neutrons are of great importance in fundamental and applied research, and neutron reflectors are an indispensable tool in this field¹⁻¹⁰. In order to design neutron reflectors that are efficient in the complete range of neutron wavelengths, new methods and materials have to be developed. Thanks to a specialized diffractometer to work with slower neutrons using the neutron beam at the PF1B instrument¹² at ILL, Grenoble, France, powdered (C₂F)_n-rich graphite fluoride with an interplanar distance *d* of 9 Å was demonstrated as an effective reflector for neutrons with wavelengths in the range 6-18 Å, completely covering the gap in the reflectivity of modern neutron reflectors¹². As a matter of fact, the efficiency of standard neutron reflectors, like graphite, decreases sharply at neutron energies below the so-called Bragg cut-off associated with the coherent scattering of neutrons on crystal planes. The value of the energy depends on the reflector material; the neutron wavelength λ_n corresponding to this energy value is equal to 2 interplanar

distances *d*. For graphite¹³, it is $\lambda_n^{Bragg(Gr)} = 2 \cdot d_{Gr} = 6.708 \text{ \AA}$, (where $d_{Gr} = 3.354 \text{ \AA}$). To overcome this limitation for the slowest neutrons, we have developed a reflector method based on fluorinated detonation nanodiamond (F-DND) powders¹⁴⁻¹⁹. Nevertheless, prior to¹², there had been still a gap in reflectivity in the neutron wavelength range $[\lambda_n^{F-DND} - \lambda_n^{Bragg}]$, only partially covered with less efficient materials²⁰. The high interplanar distance *d* (9 Å) in (C₂F)_n phase is related to stacking sequence FCCF/FCCF where half of the carbon atoms is bound to fluorine (whereas each carbon atom is fluorinated in (CF)_n phase resulting in a FCF/FCF stacking sequence with an interplanar distance equal to 6 Å. In addition to this advantage, graphite fluoride of (C₂F)_n structural phase consists of atoms with very small capture cross sections ($\sigma_{abs}^C = 3.5 \text{ mb}$ and $\sigma_{abs}^F = 9.6 \text{ mb}$ at the thermal neutron velocity, respectively) and large coherent scattering length ($b^C = 6.65 \text{ fm}$ and $b^F = 5.65 \text{ fm}$, respectively). Graphite is relatively free from impurities and can be further purified to a significant extent²¹. According to Kita's works²², GF with a (C₂F)_n phase content of 96 % was prepared using the reaction of molecular fluorine (F₂ gas) starting from flakes of natural graphite¹².

Up to now, only powders or small flakes (200-400 μm) of graphite were considered as starting materials for the fluorination²³. The next step was the compaction of the resulting GF in order to increase the density of the reflector; the higher its density, the higher its reflectivity, for the realistic geometries of reflectors. The high electronegativity of fluorine atoms appears then as a drawback because it decreases the surface energy of fluorocarbon layers and hinders the compaction. In the present work, we have chosen an alternative strategy with the fluorination of graphite foil in order to prepare GF foil with high content of (C₂F)_n. Nuclear grade was selected for the foils to avoid impurity that would increase neutron losses and be activated in high

^a Université Clermont Auvergne, ICCF, 24, avenue des Blaise Pascal, 63178 Aubière, France

^b Université de Lorraine, CNRS, Institut Jean Lamour, UMR 7198, allée André Guinier 54000 Nancy, France

^c Institut Max von Laue – Paul Langevin, 71 avenue des Martyrs, F-38042, Grenoble, France

^d Institut Lumière Matière, UMR 5306, Université de Lyon, Université Claude Bernard Lyon1, CNRS, 10 rue Ada Byron, F-69622 Villeurbanne, France

^e School of Environmental and Life Sciences, The University of Newcastle, Callaghan, New South Wales 2308, Australia.

† Footnotes relating to the title and/or authors should appear here. Electronic Supplementary Information (ESI) available: [details of any supplementary information available should be included here]. See DOI: 10.1039/x0xx00000x

radiation fluxes. The main experimental difficulty was to avoid the exfoliation of the graphite foil during the fluorination in order to maintain the density as high as possible. Because large foils are necessary for the neutron reflection, the reaction conditions must be adapted to achieve homogenous distribution of the fluorine atoms into the bulk of the foils. Unlike powder reflectors, intercalated foils provide anisotropic neutron scattering. This circumstance requires a special design to obtain an isotropic reflector. However, it opens up an additional opportunity for more efficient directional neutron scattering.

Experimental

Fluorination of graphite foil

High purity premium grade, or nuclear grade flexible graphite foils (Papyex) with thicknesses of 0.1 and 1.0 mm were kindly provided by Mersen. Following chemical preparation with acids and oxidizing agents, the natural graphite was expanded by a violent heat treatment procedure. Self-bonded by a rolling operation, the expanded graphite particles form a continuous strip, without addition of a binder. A multistep process was used to achieve ultra-low levels of sulfur (typical value 500 ppm), chloride (20 ppm, leachable chlorine content of 10 ppm) and other impurity contents. The carbon rate and ash content were 99.9 % and 0.1 %, respectively.

Our previous works on powdered $(C_2F)_n$ GF evidenced that long duration were necessary in the range 390-450°C¹². A up-scalable static mode was used to perform the fluorination for 48 h in a 5 L horizontal tubular reactor made with nickel alloy and passivated with NiF_2 . In this mode, fluorine was added in a closed reactor starting from primary vacuum. Foils of 70 x 70 mm² size and 1.0 or 0.1 mm thickness were used (see Figure 1). Before the reaction, moisture and oxygen were removed by applying a primary vacuum (10-3 mbar) at 200 °C. In order to avoid the exfoliation during addition of F_2 gas, a two-step fluorination was carried out as follows: after the preliminary step (primary vacuum at 200 °C, addition of F_2 at 270 °C, step at 360 °C for 2 h), the reaction temperature was first maintained at 390 °C for 24 h to form the $(C_2F)_n$ phase and then increased to TF (390, 410, 430 and 460 °C) to enhance the structural homogeneity by annealing. The annealing temperature was maintained for 24 h. The sample are denoted by the temperature of annealing TA and foil's thickness (0.1 or 1.0 mm), i.e. FTF-Foil0.1 and FTF Foil1.0. Addition of F_2 gas was performed when the pressure drop was at least 0.2 bar. After the fluorination and during the cooling of the reactor, the reactive atmosphere was flushed with nitrogen gas. For comparison, GF was synthesized with the same fluorination process and TA = 440 °C using natural graphite (Sigma Aldrich) with small flakes of 200-400 µm as starting material. With the same aim of comparison, a $(CF)_n$ GF was prepared at 600 °C for 3 h using graphite powder (Timrex KS4 graphite with 4 µm granulometry). Its composition is CF_1 .

Figure 1. Representative picture of the fluorinated foils (a) and cut pieces for XRD analysis (b)

{Figure 1 could be inserted here}

Graphitized graphene oxide (GO) foil was also used as starting material in order to increase the structural order and then the density. GO film was first synthesized by exfoliating graphite oxide using the modified Hummers' method^{23,24}. The resulting GO was dispersed in water to achieve a concentration of 0.5 mg mL⁻¹. GO films were prepared by vacuum-driven filtration of 10 mL of the aqueous GO dispersion through mixed cellulose ester (MCE) filters (WhatmanTM, 10401712) with a pore size of 0.2 µm and a diameter of 47 mm. Subsequently, the GO films were dried in ambient air and carefully separated from the filters by using isopropyl alcohol. To remove any residual impurities from the MCE filters, the films were washed with acetone. After the graphitization at 2750 °C, its interlayer distance was then 3.36 nm and its coherence length along the c axis was 390 Å corresponding to 116 stacked sheets. The graphenic film is carbon-pure, uniform, and flexible, with good mechanical performance, and high electrical and thermal conductivities (~1200 W m⁻¹ K⁻¹). The resulting sample is denoted gGO. Its thickness was around 0.1 mm. The same fluorination conditions than for the foils of 0.1 and 1.0 mm thickness were applied for FTF-gGO serie ($T_F = 390, 410$ and 430 °C).

Physicochemical characterization

NMR experiments were carried out with Bruker Avance spectrometer, with working frequencies for ¹³C and ¹⁹F of 73.4 and 282.2 MHz, respectively. A Magic Angle Spinning (MAS) probe (Bruker) operating with 2.5 mm rotors was used. For MAS spectra, a simple sequence was performed with a single $\pi/2$ pulse length of 4.0 and 3.5 µs for ¹⁹F and ¹³C, respectively. For MAS measurements, the samples must be grinded. ¹³C chemical shifts were externally referenced to tetramethylsilane (TMS), while ¹⁹F chemical shifts were referenced with respect to $CFCl_3$. X-ray diffraction (XRD) patterns were recorded using both a PANalytical X'PERT X-ray reflexion diffractometer with a Cu (K_{α}) radiation ($\lambda_{K_{\alpha 1}} = 1.5406$ Å) and a Bruker D8 Advance transmission diffractometer using a molybdenum anticathode ($\lambda_{K_{\alpha 1}} = 0.7093$ Å) equipped with a 2D LynxEye detector and a 2.5° divergence Soller slit. Regarding the XRD patterns recorded with Mo radiation, diffractograms were accumulated for 1 h in a 2-45° (2θ) angular range. This measurement was repeated 5 times for both (00l) and (hk0) diffractograms, in order to increase the signal-to-noise ratio. Fluorinated foil samples were placed in Lindemann glass capillaries (1.5 mm diameter). Due to the extremely oriented nature of the samples, 00l and hk0 reflections can be recorded separately depending on the orientation of samples versus the incident beam. Fourier-transform infrared (FTIR) spectra were recorded on a Nicolet 6700 FT-IR (Thermo scientific) spectrometer in transmission mode at 4 cm⁻¹ resolution and 256 scans were taken for each spectrum. Transmission electron microscopy (TEM) specimens were prepared by disintegrating the films in ethanol and drop casting the suspensions onto lacey carbon-coated Cu grids (SPI

Supplies) and dried in air. TEM analysis was performed using a JEOL JEM-F200 Multi-Purpose FEG-S/TEM operating at an accelerating voltage of 200 kV. Image J and Pathfinder were used for processing the TEM and elemental map images.

Results and discussion

In accordance with the expected value for the $(C_2F)_n$ phase ($F/C = 0.5$), a F/C molar ratio close to 0.6 was obtained by weight uptake for the GF starting whatever the temperature of fluorination and initial thickness. The composition will be extracted from ^{13}C NMR data. XRD was performed as a systematic characterization in order to study the annealing effect over the $(C_2F)_n$ structure (Figure 2). The four annealed F-Foil0.1 samples present the same XRD pattern with four diffraction peaks clearly visible (Figure 2a-b) and indexed as (001), (002), (003) and (004) planes. A magnification of the $15-70^\circ$ region is presented in Figure 2b (highlighted in yellow in Figure 2a). A shoulder is visible around 41° on the (004) peaks and corresponds to the (110) plane. It is noted that (002), (003) and (004) peaks are particularly broad, which complicates the determination of the d -space. After background subtraction, the d -space and the crystallite size along the c -axis L_c (from the full width at half maximum FWHM) were calculated precisely and the obtained values are gathered in Table 1. It is seen that the d -space increases with the annealing temperature, otherwise the FWHM and L_c do not seem to be particularly affected by the F_2 annealing. F390-Foil0.1 have a slightly lower d -space (8.41 Å) than that found in the literature (8.72-9.05 Å),^{12,26} and compared to powder with 96 % of $(C_2F)_n$ phase (9.2 Å)¹², while F460-Foil0.1 has a d -space (8.98 Å) closer to what is expected. Even through the d -space of F390-Foil0.1 is slightly lower than that expected, no other diffraction peak appears, meaning that no $(CF)_n$ pattern is necessary to fully index this diffractogram.

{Figure 2 could be inserted here}

{Table 1 could be inserted here}

The foil thickness effect on the synthesis of the $(C_2F)_n$ phase was also investigated. The (00 l) and ($hk0$) XRD patterns of F410-Foil1.0 and F410-Foil0.1 were acquired (Mo anticathode) and are respectively shown in Figures 2c and 2d. In the (00 l) XRD pattern, the same diffractograms as previously are observed and the d -space, FWHM and L_c are gathered in Table 2. Generally, the F410-Foil0.1 shows a slightly higher d -space than that observed for the 1 mm thick foil, but both samples remain quite similar. The (00 l) pattern confirms the high interlayer distance where the value is of 8.9 Å, which is in accordance with a high content of $(C_2F)_n$ phase. Nonetheless, two ($hk0$) planes are observed in the (00 l) XRD pattern: (100) at 2.18 Å ($\sim 19^\circ$) and (110) at 1.28 Å ($\sim 32^\circ$). This can be attributed to the crumpled nature of Papyex on edges with some layers being fold.

Regarding the ($hk0$) pattern (Figure 2d), three diffraction peaks are visible: (100), (110) and (200) planes at 2.17, 1.28 and 1.09

Å, respectively. As expected, no significant difference between samples can be noted regarding their initial thickness, as peak widths and positions of the $hk0$ reflections remain equivalent. The a parameter and the distance between two carbon atoms (d_{C-C}) can be extracted from the ($hk0$) planes. Thus, considering $(C_2F)_n$ an hexagonal structure³⁴, $a=2.53$ Å and $d_{C-C}=1.46$ Å compared to the a and d_{C-C} of graphite equals to 2.46 and 1.42 Å, respectively. As expected, the fluorination of graphite extends the distance between carbon atoms, increasing the in-plane lattice parameter.

{Table 2 could be inserted here}

Thus, whatever the foil thickness and more surprisingly whatever the annealing temperature in between 390 and 460 °C, the XRD patterns corresponding to fluorinated graphite can be indexed as $(C_2F)_n$ phase and no additional diffraction peak is needed to fully index the observed features. In particular, no diffraction peak corresponding to pristine graphite or $(CF)_n$ phase is noticed. Also, studying separately the ($hk0$) pattern allowed to determine the lattice parameter a and the d_{C-C} , which are higher than those of graphite.

In order to confirm the conclusion from XRD data, solid state NMR was performed for the investigation of the structural type at the short range. The ^{13}C NMR spectra of the foils fluorinated at 390 °C and annealed at 410 °C are composed of two main lines at 84 and 42 ppm which are assigned to the carbon atoms involved in the C-F bonds (denoted $\underline{C-F}$ in Figures 3a and 3d for experimental and fitting data) and non-fluorinated carbons with sp^3 hybridization ($\underline{C-C-F}$)^{27,29-32}. A very few amount of non-fluorinated sp^2 C is also evidenced by the line with a weak intensity at 135 ppm. In order to evidence CF_2 groups with an expected line at 110 ppm, $^{19}F \rightarrow ^{13}C$ cross-polarization MAS spectra were recorded. Their content is close to zero.

According to the integrated surface of the lines $S_{\underline{C-F}}$ and $S_{\underline{C-C-F}}$ (see Figure 3c for the representative example of F410-Foil0.1), the ratio $100*(C_2F)_n/(CF)_n=100*S_{\underline{C-C-F}}/S_{\underline{C-F}}$ gives the percentage of $(C_2F)_n$ structural type. 77 ± 2 % of C-F bonds are included in the $(C_2F)_n$ structural type (23 % in $(CF)_n$) for F410-Foil0.1. The F/C ratio can be extracted from the fit parameters thanks to the formula $F/C = S_{\underline{C-F}}/(S_{\underline{C-F}} + S_{\underline{C-C-F}} + S_{C_{sp^2}})$ and a value of 0.55 ± 0.01 are obtained for F410-Foil0.1 in good accordance with the weight uptake method (close to 0.6). When the initial thickness is 1.0 mm, very close results are obtained. In order to evidence the effect of the fluorination temperature, Foil0.1 was also treated at 390, 430 and 460°C, *i.e.* in the “ $(C_2F)_n$ -rich” range defined by Kita²². The data extracted from ^{13}C NMR (Fig. S11a and b in supplementary information) evidence very few differences, $\%(C_2F)_n$ is around 76% for F390-Foil0.1 and F430-Foil0.1, as for F410-Foil0.1 (see Table S11 in supplementary information). The slightly lower value of 69 ± 2 % for F460-Foil0.1 is explained by the formation of high amount of $(CF)_n$ phase but the main phase is still $(C_2F)_n$. A line at 132 ppm related to non-fluorinated carbons with C-F neighboring is observed both in MAS and ^{19}F - ^{13}C CP-MAS only for the lowest fluorination temperature of 390°C. Nevertheless, its intensity is very low. F410-Foil1.0 exhibits a F/C of 0.58 and a content of $(C_2F)_n$ phase equal to 71 %. The applied fluorination and

annealing treatment conditions were then also efficient for thicker graphite foils.

{Figure 3 could be inserted here}

Figures 3b and 3d exhibit respectively the ^{19}F experimental spectra of both F410-Foil0.1 where several lines are evidenced. The spectrum of F410-Foil0.1 was simulated as a representative example (Figure 3d). Presence of CF_2 (-120 ppm) and CF_3 (-80 ppm) is excluded regarding $^{19}\text{F} \rightarrow ^{13}\text{C}$ cross-polarization data and absence of the corresponding lines^{28,29,31}. By analogy with the chemical shift at -178 ppm of fluorinated nanodiamonds, i.e. $\text{Csp}^3\text{-C-F}$ (their ^{13}C chemical shift is also 42 ppm)¹⁵, the line at -178 ppm is related to C-F bonds in $(\text{C}_2\text{F})_n$ with only C_2F ($(\text{C}_2\text{F})_n$) neighborings (noted $(\text{C}_2\text{E})(\text{C}_2\text{F})$). The presence of $(\text{CF})_n$ phase results in the second main line at -188 ppm which is the superimposition of two components: C-F bonds in $(\text{C}_2\text{F})_n$ with CF neighboring $(\text{C}_2\text{E})(\text{CF})$ and C-F in $(\text{CF})_n$ with C-F neighboring $(\text{CE})(\text{CF})$. Finally, the shoulder at -164 ppm is assigned to C-F bonds in $(\text{C}_2\text{F})_n$ and $(\text{CF})_n$ types with non-fluorinated sp^2 carbon in their neighboring (denoted $(\text{C}_2\text{E})(\text{Csp}^2)$ and $(\text{CE})(\text{Csp}^2)$). This assignment is in the same trend as the slightly lower d-space of the samples annealed at 390, 410 and 430 °C. Because the content of $(\text{C}_2\text{F})_n$ is high regardless the fluorination temperature, the ^{19}F MAS spectra (14 kHz) are very similar to those of F390-Foil0.1, F430-Foil0.1 and F460-Foil0.1 (Fig. S11c). The assignments of the lines are similar than those of F410-Foil0.1.

Natural graphite fluorinated at 440 °C with the same reaction conditions were identified as quasi-perfect $(\text{C}_2\text{F})_n$ phase with 96 % of this phase²¹. F440-NG was used as reference and labelled $(\text{C}_2\text{F})_n$ in Figure 3. The ^{13}C and ^{19}F spectra of both foils fluorinated at 410 °C exhibit strong similarities with our reference. The characteristic lines of $(\text{C}_2\text{F})_n$ at 42 and -178 ppm for ^{13}C and ^{19}F nuclei, respectively, are of lower intensity for both F410-Foil0.1 and F410-Foil1.0 compared to the $(\text{C}_2\text{F})_n$ reference, which was expected since the $(\text{C}_2\text{F})_n$ content are lower for these samples (96 % for the F440-NG reference, 77 % for F410-Foil0.1, and 71 % for F410-Foil1.0). When compared to a typical $(\text{CF})_n$ type, these two lines are absent.

It is also interesting to compare the infrared spectra of our reference with those of F410-Foil0.1 and F410-Foil1.0. Graphite fluorides with mainly $(\text{CF})_n$ and $(\text{C}_2\text{F})_n$ phases are also considered. All infrared spectra are shown in Figure 4. The vibration of covalent C-F bond is observed at around 1200 cm^{-1} for both phases^{28,30}. The spectra with high content of $(\text{C}_2\text{F})_n$ are characterized by strong vibrational bands at 1350 and 940 cm^{-1} which are absent in $(\text{CF})_n$ type graphite fluoride. This latter band cannot be assigned to antisymmetric elongation of $>\text{CF}_2$ groups, as in the literature³², because of its high intensity. Indeed, the NMR study was not able to evidence those groups.

{Figure 4 could be inserted here}

Towards the densification of the $(\text{C}_2\text{F})_n$ graphite fluoride

To increase the density of fluorinated graphite, we prepared gGO foils with a high degree of graphitization, which were fluorinated under the same conditions than those used previously to promote the formation of the $(\text{C}_2\text{F})_n$ phase. The shape/size of the foils remained unchanged after fluorination at all tested temperatures (Figure 5a). However, we noted that the sub-metallic appearance was lost after fluorination, resulting in a greyish color for the FTF-gGO series. Despite this change, the mechanical properties were maintained, and the foils did not become more fragile after treatment. XRD analysis revealed interlayer distances of 8.2 Å and 8.1 Å for F390-gGO and F410-gGO, respectively (Figure 5b). These values are slightly lower than the expected interlayer distance for the $(\text{C}_2\text{F})_n$ phase (9 Å). The conversion of $(\text{C}_2\text{F})_n$ into $(\text{CF})_n$ phase is favored in the case of F430-gGO as revealed by the interlayer distance of 7.0 Å, which is closer to the value expected for $(\text{CF})_n$ (6 Å). IR spectra (Figure 5c) further confirmed the high content of the $(\text{C}_2\text{F})_n$ phase, with prominent bands at 1350 cm^{-1} and 940 cm^{-1} , in addition to the main band at 1200 cm^{-1} . F390-gGO showed singularities with an inclined baseline, an additional line at 964 cm^{-1} , and a shoulder at 1110 cm^{-1} , indicating the presence of non-fluorinated carbon with sp^2 hybridization. The line at 964 cm^{-1} is typically present when two conditions are met: the presence of a $(\text{C}_2\text{F})_n$ phase and a significant amount of sp^2 C^{12} . While IR spectroscopy data confirmed the high content of the $(\text{C}_2\text{F})_n$ phase, it was unable to estimate the corresponding content accurately. Solid-state NMR analysis of FTF-gGO required milling, which could be destructive. To avoid this approach, an alternative method was employed. By utilizing the linear relationship between the intensity ratio I_{940}/I_{1200} ²¹ as a function of the percentage of $(\text{C}_2\text{F})_n$ phase, this latter value could be graphically deduced. F410-gGO and F430-gGO exhibited percentages of $(\text{C}_2\text{F})_n$ phase equal to 52 % and 46 %, respectively. As expected from XRD data, this content is lower for F430-gGO because of the higher conversion into $(\text{CF})_n$ phase. However, this method was not suitable for F390-gGO due to both the non-zero baseline and the shoulder at 1100 cm^{-1} . The F/C ratio, i.e. $\text{F/C} = x$ in CF_x , can be calculated as $\text{F/C} = 1/(1 + \%(\text{C}_2\text{F})_n)$; the values are 0.66 and 0.68 for F410-gGO and F430-gGO, respectively.

{Figure 5 could be inserted here}

Figure 6a shows a TEM image of a typical exfoliated platelet from F410-gGO with the highest $(\text{C}_2\text{F})_n$ content in the series, i.e. 52 %. A magnified TEM image (Figure 6b), from the indicated area in Figure 6a, shows the edge of the platelet, with a further zoomed-in image in Figure 6c showing the presence of 5-6 layers. Figure 6d shows a plot of profile along the line in Figure 6c. The distance between the two dotted lines is ~27 Å, indicating an average interlayer distance of ~9 Å within the lattices, consistent with the expected interlayer distance for the $(\text{C}_2\text{F})_n$ phase. Another platelet was observed (Figure 6e), where a high-angle annular dark-field (HAADF) image acquired using the scanning transmission electron microscopy (STEM) mode (Figure 6f) was acquired and corresponding elemental maps of carbon and fluorine were performed (Figure 6g and 6h). These maps indicate a uniform presence of carbon and fluorine within the exfoliated $(\text{C}_2\text{F})_n$.

{Figure 6 could be inserted here}

Conclusions

Using a minute control of the fluorination conditions, the partial exfoliation of graphite foil was avoided whatever their initial thickness, 0.1 or 1.0 mm. Long duration fluorination (24 h) at 390 °C followed by an annealing (24 h) at 410 °C under pure F₂ gas for the same time allowed homogenous fluorination to be achieved. The higher content of (C₂F)_n phase, i.e. 56 %, was achieved at 430 °C for thinner (0.01 mm) graphitized GO foil. Keeping the temperature in the “(C₂F)_n rich domain” defined by Kita et al²², high content of this phase was obtained for the two types of foils, i.e. 77 and 71 % for graphite foils of 0.1 and 1.0 mm thicknesses. Those percentages of (C₂F)_n phase (%(C₂F)_n) were extracted from ¹³C NMR data whereas the values for FFT-gGO series were estimated with the linear relationship between the IR intensity ratio I₁₃₄₀/I₁₂₀₀ and %(C₂F)_n²². All the samples prepared exhibit then an IR spectrum typical of (C₂F)_n phase, i.e. with 3 bands at 1350, 1200 and 940 cm⁻¹. Those features resulted in an interlayer distance d close to 9 Å for the 0.1 and 1.0 mm thickness foils (8.6 for FTF-gGO series) Furthermore, the content of non-fluorinated sp² carbons was very low regarding ¹³C NMR data. All these characteristics made the fluorinated graphite foils with mainly (C₂F)_n structural phase very promising as reflector for slow neutrons. As evidenced by ¹⁹F NMR spectra, a substantial (CF)_n phase was observed in all samples, indicating that the (C₂F)_n regions were surrounded by (CF)_n ones which then participate to the XRD patterns of the samples (interlayer distance of 6 Å). Nonetheless, the average d value was close to 9 Å, slightly lower, as targeted. Graphite fluorides under the form of flexible foils of (C₂F)_n structural phase are efficient reflectors for neutrons with wavelengths higher than $\lambda_n^{Bragg(Gr)12}$. Moreover, the flexibility of the foils was maintained after fluorination that allowed to build curved walls with the prepared fluorinated graphite foils for the desired slow neutron reflectors.

Author Contributions

Investigation was mainly performed by Killian Henry, with help of Marc Dubois, Brigitte Vigolo, Claire Herold and Sébastien Cahen. Marie Colin, Gabin Chambéry, Valery Nesvizhevsky, Sylvie Le Floch, Vittoria Pischedda and Sam Chen have contributed for fluorination, characterization, neutron science, high pressure measurements, high pressure measurements too and works on GO membranes, respectively. Writing – original draft was performed by Marc Dubois and Killian Henry by adding also parts from Valery Nesvizhevsky and Sam Chen. Writing – review & editing was performed by Marc Dubois and Sébastien Cahen. All authors have given approval to the final version of the manuscript.

Conflicts of interest

There are no conflicts to declare.

Acknowledgements

We are grateful to Mersen for providing the graphite foils (Papyex). The authors are grateful to ANR for the funding of this work with the project NERF (ANR-20-CE08-0034). The authors would like to thank the platform “X-Gamma” at the Institut Jean Lamour (IJL, Nancy, France) for XRD facilities access.

Notes and references

- I. Halpern, E. Fermi. Neutron Physics. s.l. : Los Alamos, 1946.
- V.F. Sears. Neutron Optics. New York - Oxford : Oxford Univ. Press, 1989.
- B.T.M. Willis, C.J. Carlile. Experimental Neutron Scattering. Oxford : Science, 2009.
- A. Furrer, J. Mesot, Th. Strassle. Neutron Scattering in Condensed Matter Physics. London : World Scientific, 2009.
- S. Esposito, O. Pisanti. Neutron Physics for Nuclear Reactors. Unpublished. Writings by Enrico Fermi. London : World Scientific, 2010.
- D. Dubbers, M.G. Schmidt. The neutron and its role in cosmology and particle physics. *Rev. Mod. Phys.* 83 (2011) 1111. <https://doi.org/10.1103/RevModPhys.83.1111>
- F.E. Wietfeldt, G.L. Greene. Colloquium: the neutron lifetime. *Rev. Mod. Phys.* 2011, **83**, 1173. <https://doi.org/10.1103/RevModPhys.83.1173>
- V.V. Nesvizhevsky. The discovery of the neutron and its consequences (1930–1940). *Compt. Rend. Phys.* 18 (2017) 592–600. <https://doi.org/10.1016/j.crhy.2017.11.001>
- W.H. Bragg, W.L. Bragg. The reflection of X-rays by crystals. *Proc. Royal Soc. London A.* 1913, **88**, 428. <https://doi.org/10.1098/rspa.1913.0040>
- E. Fermi, Experimental production of a divergent chain reaction. *Amer. J. Phys. S.* 1952, **20**, 536. <https://doi.org/10.1119/1.1933322>
- H. Abele, D. Dubbers, H. Hase, M. Klein, A. Knopfler, M. Kreuz, T. Lauer, B. Markisch, D. Mund, V. Nesvizhevsky, A. Petoukhov, C. Schmidt, M. Schumann, T. Soldner. Characterization of a ballistic supermirror neutron guide. *Nucl. Instr. Meth. A.* 2006, **562**, 407–417. <https://doi.org/10.1016/j.nima.2006.03.020>
- V. Nesvizhevsky, K. Henry, L. Dauga, B. Clavier, S. Le Floch, A. Muzychka, A. Nezvanov, V. Pischedda, C. Tender, K. Turlybekuly, S. Radescu, B. Vigolo, S. Cahen, C. Hérold, J. Ghanbaja, M. Dubois, Carbon, under review
- M. Utsuro, K. Inoue. Bragg cutoff effects on neutron wave propagation in graphite. *J. Nucl. Sci. Techn.* 1968, **5**, 298–308. <https://doi.org/10.1080/18811248.1968.9732458>
- V.V. Nesvizhevsky, Interaction of neutrons with nanoparticles. *Phys. At. Nucl.* 2002, **65**, 400–408.
- V.V. Nesvizhevsky, E.V. Lychagin, A.Yu. Muzychka, A.V. Strelkov, G. Pignol, K.V. Protasov. The reflection of very cold neutrons from diamond powder nanoparticles. *Nucl. Instr. Meth. A.* 2008, 2008, **595**, 631–636. <https://doi.org/10.1016/j.nima.2008.07.149>
- E.V. Lychagin, A.Yu. Muzychka, V.V. Nesvizhevsky, G. Pignol, K.V. Protasov, A.V. Strelkov. Storage of very cold neutrons in a trap with nano-structured walls. *Phys. Lett. B.* 2009, **679**, 186–190. <https://doi.org/10.1016/j.physletb.2009.07.030>
- V. Nesvizhevsky, U. Koster, M. Dubois, N. Batisse, L. Frezet, A. Bosak, L. Gines, O. Williams. Fluorinated nanodiamonds as unique neutron reflector. *Carbon.* 2018, **130**, 799–805. <https://doi.org/10.1016/j.carbon.2018.01.086>
- A. Bosak, A. Dideikin, M. Dubois, J. Ivankov, E. Lychagin, A. Muzychka, G. Nekhaev, V. Nesvizhevsky, A. Nezvanov, R. Schweins, A. Strelkov, A. Vul', K. Zhernenkov. Fluorination of diamond nanoparticles in slow neutron reflectors does not destroy their crystalline cores and clustering while decreasing neutron losses. *Mater.* 2020, **13**, 3337. <https://doi.org/10.3390/ma13153337>
- A. Aleksenskii, M. Bleuel, A. Bosak, A. Chumakova, A. Dideikin, M. Dubois, E. Korobkina, E. Lychagin, A. Muzychka, G. Nekhaev, V. Nesvizhevsky, A. Nezvanov, R. Schweins, A. Shvidchenko, A. Strelkov, K. Turlybekuly, A. Vul', K. Zhernenkov. Effect of particle sizes on the efficiency of fluorinated nanodiamond neutron reflectors. *Nanomater.* 2021, **11**, 3067. <https://doi.org/10.3390/nano11113067>

20. J.R. Granada, J.I.M. Damian, J. Dawidowski, J.I. Robledo, C. Helman, G. Romanelli, G. Skoro. Development of neutron scattering kernels for cold neutron reflector materials. *J. Neutron Res.* 2021, **23**, 167.
21. K. Shen, X. Chen, W. Shen, Z.-H. Huang, B. Liu. Thermal and gas purification of natural graphite for nuclear. *Carbon* 2021, **173**, 769. <https://doi.org/10.1016/j.carbon.2020.11.062>
22. Y. Kita, N. Watanabe, Y. Fujii. Chemical Composition and Crystal Structure of Graphite Fluoride. *J. American Chem. Soc.* 1979, **101**, 3832-41. <https://doi.org/10.1021/ja00508a020>.
23. W.S. Hummers, R.E. Offeman Preparation of graphitic oxide *J. Am. Chem. Soc.*, 80 (6) (1958), p. 1339, 10.1021/ja01539a017
24. N.I. Kovtyukhova, P.J. Ollivier, B.R. Martin, T.E. Mallouk, S.A. Chizhik, E.V. Buzaneva, A.D. Gorchinskiy. Layer-by-Layer assembly of ultrathin composite films from micron-sized graphite oxide sheets and polycations. *Chem. Mater.*, 1999, **11** (3), 771-778, <https://doi.org/10.1021/cm981085u>
25. X. Chen, X. Deng, N. Y. Kim, Y. Wang, Y. Huang, L. Peng, M. Huang, X. Zhang, X. Chen, D. Luo, B. Wang, X. Wu, Y. Ma, Z. Lee, R. S. Ruoff, Graphitization of graphene oxide films under pressure, *Carbon* 2018, **132**, 294-303. <https://doi.org/10.1016/j.carbon.2018.02.049>.
26. Y. Sato, K. Itoh, R. Hagiwara, T. Fukunaga, Y. Ito. Short-range structures of poly(dicarbon monofluoride) (C₂F)_n and poly(carbon monofluoride) (CF)_n. *Carbon* 2004, **42**, 2897-2903. <https://doi.org/10.1016/j.carbon.2004.06.042>.
27. T. Mallouk, N. Bartlett, Reversible intercalation of graphite by fluorine: a new bifluoride, C₁₂HF₂, and graphite fluorides, C_xF (5 > x > 2) *J. Chem. Soc., Chem. Commun.* 1983, 103-105. <https://doi.org/10.1039/C39830000103>
28. T. Mallouk, B. L. Hawkins, M. P. Conrad, K. Zilm, G. E. Maciel, N. Bartlett, Raman, infrared and n.m.r. studies of the graphite hydrofluorides C_xF_{1-δ}(HF)_δ (2 ≤ x ≤ 5) *Philos. Trans. R. Soc.* 1985, **314**, 179. <https://doi.org/10.1098/rsta.1985.0017>
29. M. Dubois, J. Giraudet, K. Guérin, A. Hamwi, Z. Fawal, P. Pirotte, F. Masin, EPR and Solid-State NMR Studies of Poly(dicarbon monofluoride) (C₂F)_n *J. Phys. Chem. B* 2006, **110**, 11800-11808. <https://doi.org/10.1021/jp061291m>
30. J. Giraudet, M. Dubois, K. Guérin, C. Delabarre, A. Hamwi, F. Masin, Solid-State NMR Study of the Post-Fluorination of (C_{2.5}F)_n Fluorine-GIC *J. Phys. Chem. B* 2007, **111**, 14143-14151. <https://doi.org/10.1021/jp076170g>
31. M. Dubois, J. Giraudet, K. Guérin, A. Hamwi, Z. Fawal, P. Pirotte, F. Masin, EPR and Solid-State NMR Studies of Poly(dicarbon monofluoride) (C₂F)_n *J. Phys. Chem. B* 2006, **110**, 24, 11800-11808
32. H. Touhara, K. Kadono, Y. Fujii, N. Watanabe, On the Structure of Graphite Fluoride, *Z. Anorg. Allg. Chem.* 1987, **544**, 7-20. <https://doi.org/10.1002/zaac.19875440102>.

ARTICLE

Table 1. $d_{(hkl)}$ (in Å), FWHM (°) and Lc for the (001) peak (in Å) of the four annealed FT_A-Foil0.1 samples ($T_A = 390, 410, 430$ and 460 °C). The XRD patterns were acquired using a Cu K α_1 source ($\lambda = 1.5406$ Å)

	F390-Foil0.1			F410-Foil0.1			F430-Foil0.1			F460-Foil0.1		
	$d_{(001)}$ (Å)	FWHM (°)	Lc ₍₀₀₁₎ (Å)	$d_{(001)}$ (Å)	FWHM (°)	Lc ₍₀₀₁₎ (Å)	$d_{(001)}$ (Å)	FWHM (°)	Lc ₍₀₀₁₎ (Å)	$d_{(001)}$ (Å)	FWHM (°)	Lc ₍₀₀₁₎ (Å)
(001)	8.41	3.41	24.4	8.63	3.62	22.0	8.63	3.54	22.5	8.90	3.48	22.9
(002)	4.35	4.08	-	4.48	4.27	-	4.53	3.73	-	4.59	4.46	-
(003)	2.91	3.93	-	2.95	4.06	-	2.95	4.18	-	2.94	3.79	-
(004)	1.97	-	-	1.98	-	-	1.98	-	-	1.98	-	-

Table 2. Comparison of $d_{(hkl)}$ (in Å), FWHM (°) and Lc (in Å) between F410-Foil0.1 and F410-Foil1.0. The XRD patterns were acquired using a Mo K α_1 source ($\lambda = 0.7093$ Å)

	F410-Foil0.1			F410-Foil1.0		
	$d_{(001)}$ (Å)	FWHM (°)	Lc ₍₀₀₁₎ (Å)	$d_{(001)}$ (Å)	FWHM (°)	Lc ₍₀₀₁₎ (Å)
(001)	8.90	1.41	26.0	8.80	1.27	28.8
(002)	4.50	2.07	-	4.33	1.92	-
(003)	2.95	1.74	-	2.97	1.86	-
(004)	1.99	-	-	1.99	-	-

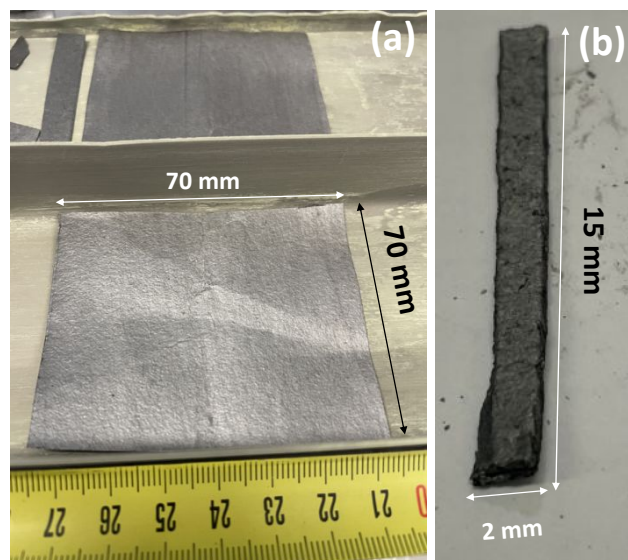


Figure 1. Representative picture of the fluorinated foils (a) and cut pieces for XRD analysis (b)

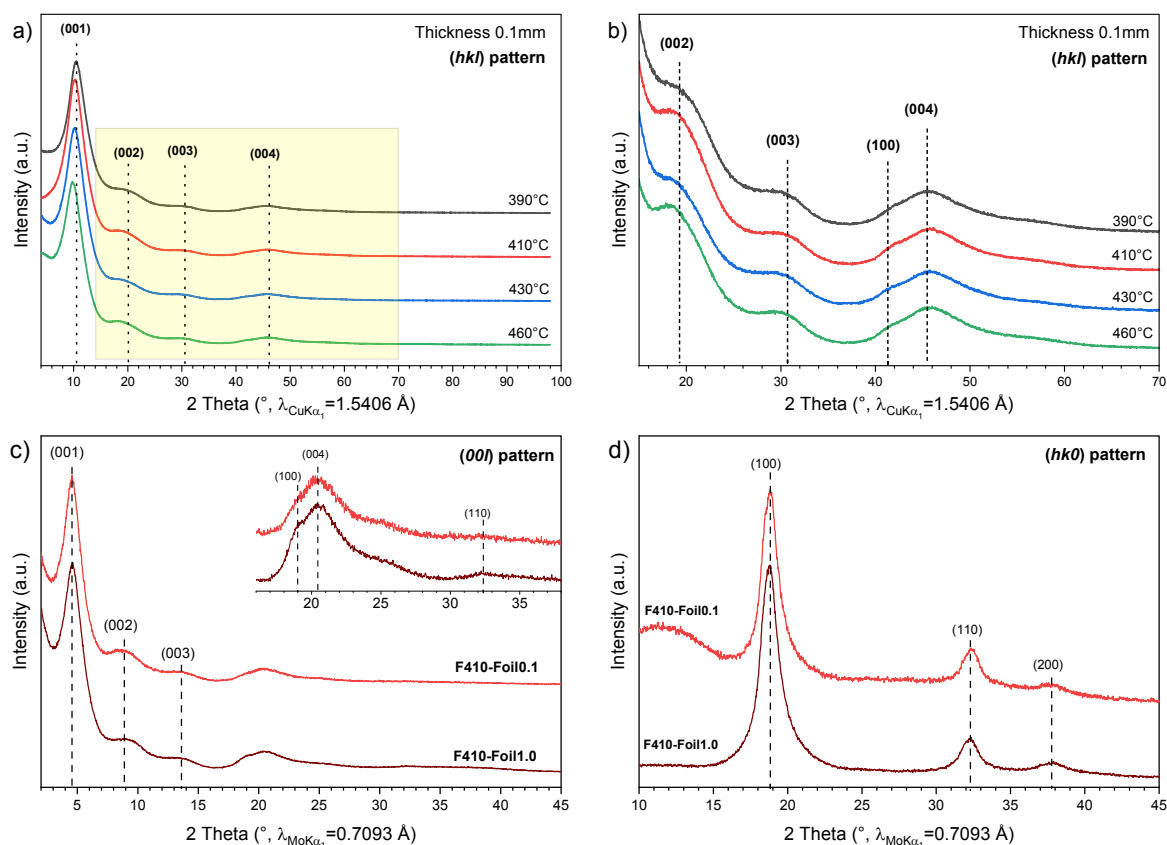


Figure 2. (a) XRD patterns of fluorinated graphite foils (Cu $K\alpha$ radiation with $\lambda_{K\alpha 1} = 1.5406 \text{ \AA}$) and (b) being a magnification of the 15-70° 2θ range (shown as a yellow area on (a)). (c) and (d) are respectively the (00l) and (hk0) patterns of foils of 0.1 (F410-Foil 0.1, red) and 1.0 mm (F410-Foil1.0, dark red) thick fluorinated at 390 °C and then annealed under F_2 gas at 410 °C. The latter were acquired with a Mo $K\alpha$ source ($\lambda_{K\alpha 1} = 0.7093 \text{ \AA}$).

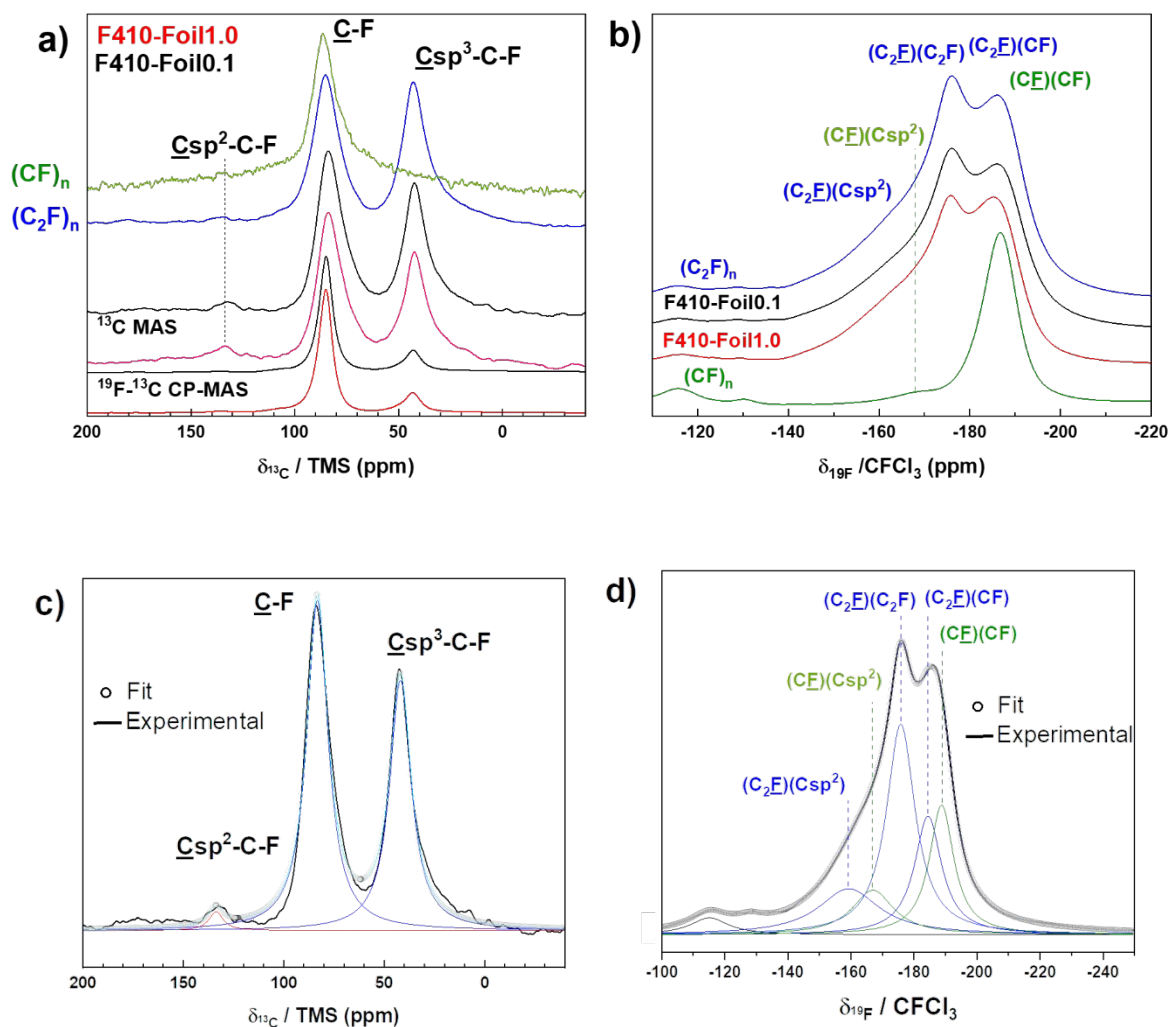


Figure 3. MAS NMR spectra of F410-Foil0.1 (black line) and F410-Foil1.0 (red line) on ^{13}C (a) and ^{19}F nuclei (b). The spinning rates are 10 and 30 kHz, respectively. Sample F440-NG from [Error! Bookmark not defined.] is used as a $(\text{C}_2\text{F})_n$ reference for both ^{13}C and ^{19}F spectra (in blue). The spectra of a $(\text{CF})_n$ reference were added (in green). Representative examples of fits for ^{13}C (c) and ^{19}F (d) spectra are shown (F410-Foil0.1).

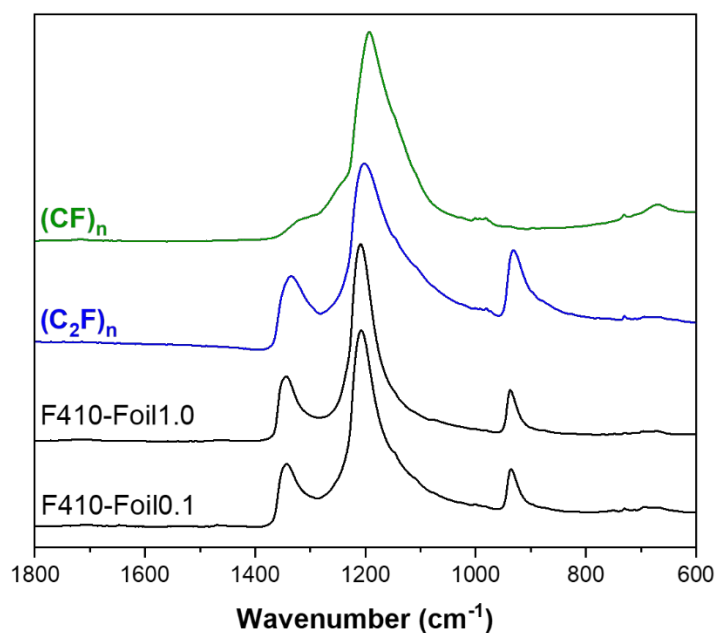


Figure 4. IR spectra of fluorinated graphite foils (0.1 and 1.0 mm annealed at 410 °C) and reference compounds of both $(C_2F)_n$ (F440-NG sample) and $(CF)_n$ structural types.

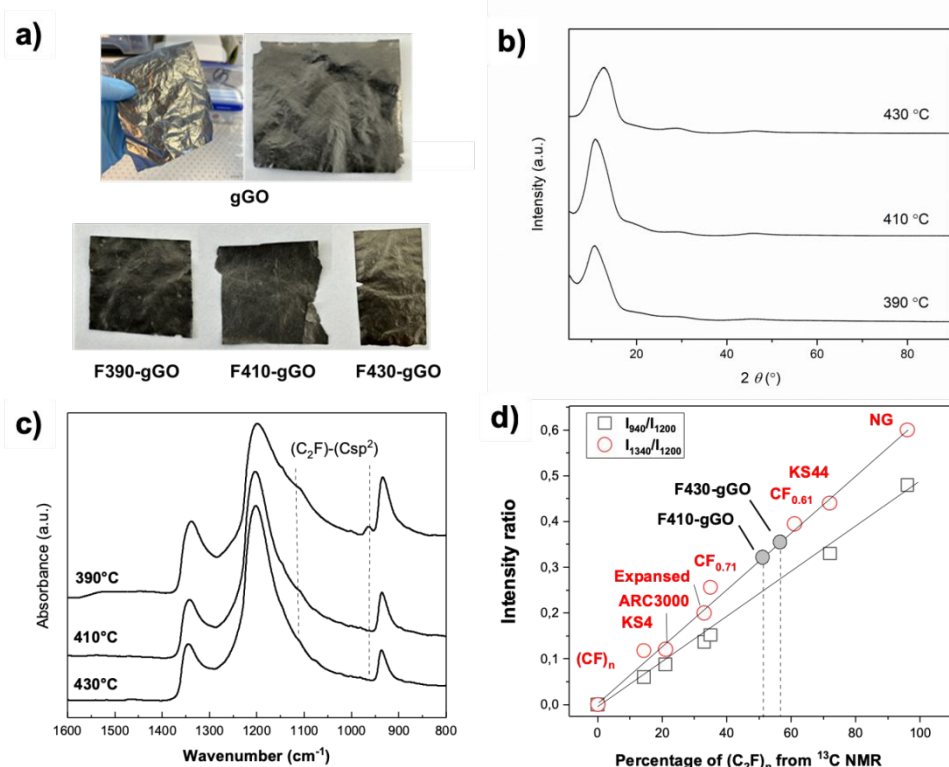


Figure 5. Photographs of gGO foils before and after fluorination (a). XRD patterns of fluorinated gGO foils (b). IR spectra of the fluorinated gGO films. The intensity ratio of the lines typical of $(C_2F)_n$ phase as

a function of the percentage of $(C_2F)_n$ phase from ^{13}C NMR is plotted in d). The CF_x compositions in a) are extracted by the weight uptake method.

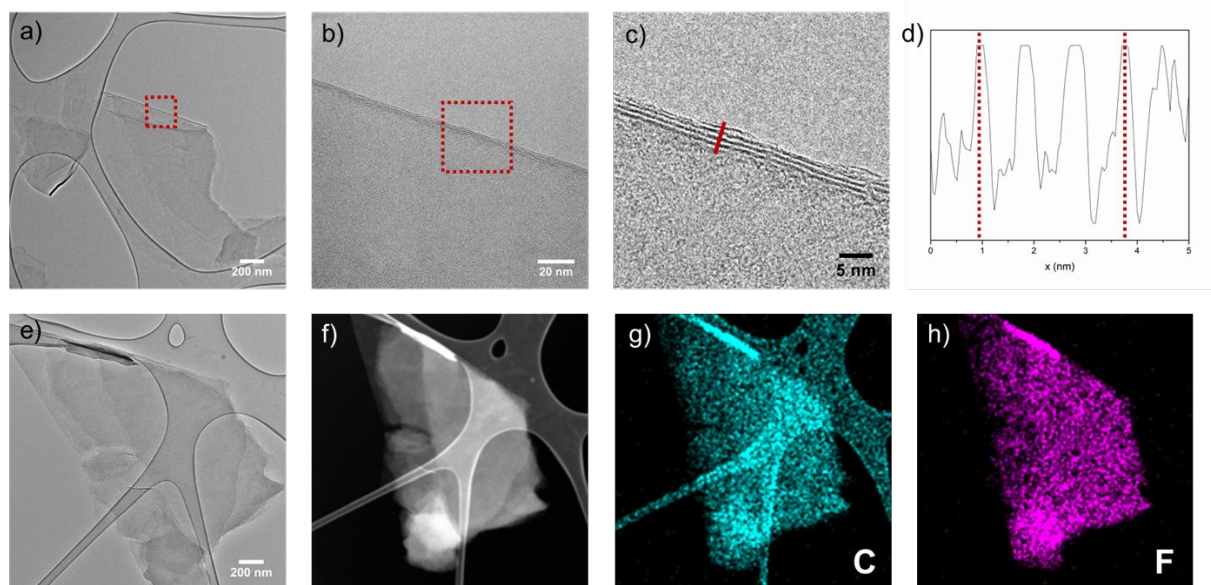


Figure 6. (a) TEM image of a typical exfoliated platelet from F410-gGO. (b) Magnified TEM image from the indicated area in (a), showing the edge of the platelet. (c) Further magnified TEM image from the indicated area in (b), with (d) showing a plot of the profile along the line in (c). (e) TEM image of another exfoliated platelet from F410-gGO, with (f) showing the corresponding STEM-HAADF image and (g, h) showing the elemental maps of C and F.